MASS TRANSPORT PHENOMENA IN MICROGRAVITY

PRELIMINARY RESULTS OF THE FIRST MEPHISTO FLIGHT EXPERIMENT

J. J. Favier, J. P. Garandet, A. Rouzaud and **D. Camel**

Commissariat à l'Energie Atomique
DTA/CEREM/DEM/SESC
Centre d'Etudes Nucléaires de Grenoble, 85X 38041 Grenoble Cedex

ABSTRACT

The MEPHISTO space program is the result of a cooperative effort that involves the French nuclear and space agencies (Commissariat à l',energie atomique, CEA - Centre National d'Etudes Spatiales, CNES) and the American National Aeronautics and Space Administration (NASA). The scientific studies and apparatus development were funded in the frame of the GRAMME agreement between CEA and CNES, the flight costs being taken in charge by NASA. Six flight opportunities are scheduled, with alternating French and American principal investigators. It is the purpose of this paper to briefly present MEPHISTO (more details can be found in refs. [1,2]) along with the preliminary results obtained during its first flight on USMP-1 in October 1992.

INTRODUCTION

The MEPHISTO space program is the result of a cooperative effort that involves the French nuclear and space agencies (Commissariat à l'énergie atomique, CEA - Centre National d'Etudes Spatiales, CNES) and the American National Aeronautics and Space Administration (NASA). MEPHISTO is basically a directional solidification furnace, where three samples are simultaneously processed. An original point is that there are in fact two heating/cooling subsystems (see fig. 1); one of them is maintained at a fixed position to provide a reference interface, whereas the other is allowed to move for solidification and melting of the samples. Only low melting point materials can be used in the furnace, its maximum temperature being presently 1000°C. The first flight featured bismuth doped tin alloys (Sn : 0.5% at. Bi), the second, scheduled for April 1994 with Prof. Abbaschian of the University of Florida as principal investigator, will focus on the other side of the phase diagram, i.e. tin doped bismuth alloys.

Sample #1 is dedicated to a measure of the Seebeck voltage between the two ends; we shall later come back in detail on the interpretation of the signal. At this point, we shall only state that the system acts as its own thermocouple, with a "cold" and a "hot" reference junction (respectively the

moving and fixed interfaces). The Seebeck voltage is then a measure of the undercooling at the growth front, a key feature being that the signal is obtained in real time. It is thus possible to run many experimental cycles on the same sample, which in turn allows to check the reproductibility of the process and to ensure a better accuracy of the results.

On sample #2, the position and the velocity of the moving interface are obtained from an on line resistance measurement. At the end of the experimental cycle, a quench freezes the structure of the solid-liquid front. Peltier pulse marking performed on sample #3 allow the determination of the shape of the interface at given time intervals. Moreover, thermocouples present in the liquid phase for both samples #2 and #3 are used to determine the temperature gradient and possible thermal fluctuations.

During the first flight, experiments were carried out both below and above the morphological stability threshold. As for the contents of this paper, sections I and II are respectively dedicated to the presentation of the planar and cellular front results. Since the metallographic analyses are not completed yet, we shall focus on the analysis of the Seebeck signals that were shown to correlate well with a *posteriori* concentration measurements in the solid phase [1].

I. PLANAR FRONT GROWTH

Undercooling with respect to the equilibrium temperature is a necessary driving force for solidification; it depends on a variety of process parameters, e.g. growth rate, convection level in the melt, partition ratio. Let us now see how it can be related to the Seebeck voltage; to do so, we have to consider the local thermoelectricity equation:

$$E = j / \sigma + \eta \nabla T \tag{1}$$

that relates electric field and current (E, j), electrical conductivity (σ), thermoelectric power (η) and temperature gradient (∇T). The MEPHISTO loop is schematized in fig. 2, the two solid parts being connected by a liquid bridge. No net current is allowed across a given section, that is:

$$\int_S j \cdot dS = 0 \tag{2}$$

Assuming that both interfaces are planar and that the thermoelectric powers of the liquid and the solid remain constant around the melting temperature, integration all over the sample leads to (see for instance [1,2]):

$$E_s = \left(\eta_s - \eta_L \right)\left(T_1 - T_{eq} \right) \tag{3}$$

The observed Seebeck voltage is thus proportional to the difference between the temperatures of the moving and fixed -equilibrium- interfaces. We shall see later on, when we deal with cellular interfaces,

28

that the integration of eq. (1) is much more complicated. At this point however, the reader should keep in mind that the thermoelectric powers of liquid and solid tin near the melting temperature are very close, $\eta_s - \eta_L \approx 1.6 \mu v / K$. We thus have to deal with very low signals, ranging typically from 0.1 to 5 μV.

Shown in fig. 3 are two typical Seebeck results of the flight experiment obtained at solidification velocities of 5.2 and 2 $\mu m/s$. After an initial transient - longer for the lower growth rate - the curves reach a plateau and the undercooling falls back to zero when the pulling is stopped. Since both plateau appear to be at the same level, it may be thought that mass transfer during solidification was principally diffusive. It is indeed well known that convection in the melt is greatly reduced in microgravity experiments; however it may still have a significant influence on solute transport, specially at low growth velocities.

To check this important point, we relied on a scaling analysis approach. We shall not dwell on the theoretical basis of the method, the interested reader being here referred to Lin and Segel [3]. Briefly stated, the purpose of such an analysis is to identify the relevant non dimensional parameters of a given problem and to obtain order of magnitude relationships between them. This method was applied to the study of solute repartition in crystal growth configurations [4], and the agreement with existing numerical data was found to be very good [5,6].

The problem was seen to depend on the value of the Peclet number, $Pe = HV_l / D$, H being the inner diameter of the crucible, V_l the growth rate and D the diffusion coefficient. Also of importance is the product of the Grashof (Gr) and Schmidt (Sc) numbers, defined as:

$$Gr = \beta_T \ g \ G_L \ H^4 / v^2 \qquad\qquad Sc = v / D$$

In the above expression, β_T is the thermal expansion coefficient, g the intensity of gravity, G_L the temperature gradient normal to g and v the kinematic viscosity of the fluid.

Moreover, an experimental validation was obtained from ground based studies in the frame of the MEPHISTO program. In fig. 4, the variation of the nondimensional parameter Δ, that measures the relative influence of diffusion and convection on mass transfer (see for instance [7]), is plotted versus Pe. For ground based experiments in bismuth and lead doped tin alloys, we had $Gr = 5.7 \times 10^4$ and $Sc = 144$. A good agreement was observed for both convective (low Pe, $\Delta \approx 0$) and diffusive (high Pe, $\Delta \approx 1$) mass transfer conditions.

Having gained confidence in the validity of the scaling analysis, we proceeded to apply it to the flight configuration. Considering the average "steady" background accelerations to be of the order of $10^5 \ g_0$, we found:

$$V_l = 2 \ \mu m/s \qquad\qquad \Delta = 0.98$$
$$V_l = 5.2 \ \mu m/s \qquad\qquad \Delta = 1$$

These high values of Δ are characteristic of very weak convective solute transport. A further confirmation was obtained applying the numerical method developed by Rouzaud [8] to solve the coupled heat/mass transfer Stefan problem. Taking the diffusion coefficient of Bi as a free parameter, the best fit was observed for the published value, $D = 1.8 \times 10^{-9}$ m^2 /s (see fig. 5).

It can thus be confidently stated that solute transport was indeed diffusive during the MEPHISTO flight experiment. However, one should keep in mind that convection may play a significant role even in microgravity. Indeed, for a pulling velocity of 0.5 μm/s, the scaling analysis predicts a value of $\Delta = 0.71$, quite far away from unity. Moreover, transient effects (g-jitters) can also disrupt the diffusive regime.

Shown in fig. 6 is the response of the Seebeck signal to a major gravity perturbation (OMS burn) that occurred during the initial part of the USMP-1 mission. A significant variation of undercooling is observed, and the return to the steady regime is very slow. The numerical studies of Alexander et al. [9,10] indeed predicted important decay periods, but more work is certainly necessary to quantify the effect of g jitters during solidification.

II. CELLULAR GROWTH

As the pulling velocity is increased, the planar front becomes unstable; this is the well known morphological stability problem, first treated by Rutter and Chalmers [11]. Their approach was later refined by Mullins and Sekerka [12], and a lot of papers on the topic have been published in the past 30 years (see for instance [13,14]). Briefly stated, the thermal gradient at the solid liquid front G and the growth rate V are the key variables of the problem.

The critical interface velocity can be experimentally estimated following the Seebeck voltage on MEPHISTO. Indeed, we just saw that for planar front, diffusive conditions, the undercooling did not depend on the pulling rate. We shall soon come back on the interpretation of the Seebeck signal in cellular growth, but at this point we can assume that any departure from the plateau value will be characteristic of the morphological instability.

Shown in fig. 7 is the variation of the undercooling as a function of growth rate measured during the USMP-1 mission. A clear rupture is observed around $V_I{}^C = 21 \pm 2$ mm/hr. Let us now apply Mullins and Sekerka standard analysis,

$$\frac{\overline{G}}{V_I^c} = \frac{m_L}{D} \frac{1-k}{k} C_o \, S(A)$$

(4)

where $\overline{G}$ is the average temperature gradient at the solid-liquid front, V_I is the growth rate, m_L is the slope of the liquidus, k the partition coefficient and C_0 the nominal Bi concentration of the alloy. S(A) is a correction factor accounting for capillarity phenomena. Using the growth parameters listed in table 1, we find: $V_I{}^C = 23.8$ mm/hr. V thus derived is slightly higher than the experimental value. However,

some of the variables of the problem (e.g. C_O and G_L) will have to be accurately measured before a definite conclusion can be drawn.

When the pulling velocity is further increased, the narrow cells formed at the onset of morphological instability will elongate and finally turn into dendrites at high growth rates. In that case, the interpretation of the observed Seebeck voltage becomes more difficult; since we here propose a first tentative explanation, we shall proceed quite slowly. As done for the planar front case, integration of eq. (1) along a line parallel to the sample axis and over the cross section yields:

$$\frac{1}{S}\int_S \int_L E.dL\, dS \;=\; E_s \tag{5}$$

Again, considering the second term in eq. (1), a contribution to the signal similar to that of planar front conditions is obtained:

$$\frac{1}{S}\int_S \int_L \eta \nabla T \cdot dl\, dS \;=\; (\eta_s - \eta_L)\left(\frac{1}{S}\int_S T_1(x,y)dS - T_{eq}\right) \tag{6}$$

The first term in the bracket on the right hand side of eq. 6) simply represents the average temperature of the moving interface.

The main difference with the planar front case is that local thermoelectric currents (first term in eq. (1), see fig. 8a) may contribute significantly to the signal. In order to gain some insight into this problem, we considered an idealized, rectangular wave interface, the temperatures at the top and the bottom of the structure -of thickness z_B - being respectively T_T and T_B (see fig. 8b). Such a model can be used to describe qualitatively a cellular growth front, the main restriction being that the liquid surface fraction f_L is not allowed to vary along the cells.

Following the approach initially proposed by Alboussiere et al. [15], let us consider a local current loop in fig. 8b. If the model cells are sufficiently long for j to follow the sample axis, the integration of the $1/\sigma$ j.dl term along the loop becomes straightforward:

$$\int \frac{1}{\sigma}j.dl \;=\; z_B\left(\frac{j_s}{\sigma_s} - \frac{j_L}{\sigma_L}\right) = -\eta_s(T_T - T_B) - \eta_L(T_B - T_T) \tag{7}$$

If we further assume the current density to be uniform both within the liquid and the solid, we get from eq. (2):

$$f_L\, j_L + f_s\, j_s \;=\; 0 \tag{8}$$

Eqs. (7) and (8) determine the current densities in the liquid and the solid; integration over the cross section and along the structure then yields:

$$\frac{1}{S}\int_S \int_L \frac{1}{\sigma}\, j.dl\ dS \ = \ -(\eta_s - \eta_L)f_L f_S(\sigma_L - \sigma_S)\left(\frac{1}{f_L\sigma_L + f_S\sigma_S}\right)(T_T - T_B) \tag{9}$$

Using the same rectangular wave growth front in the temperature term (eq. (6)), we find :

$$\frac{1}{S}\int_S \int_L \eta \nabla T.dl\ dS \ = \ (\eta_s - \eta_L)\left[f_S(T_T - T_{eq}) + f_L(T_B - T_{eq})\right] \tag{10}$$

Combining eqs. (9) and (10), we finally get for the Seebeck voltage across the sample :

$$E_S \ = \ (\eta_s - \eta_L)\left[(T_T - T_{eq}) + \frac{f_L\sigma_L}{f_L\sigma_L + f_S\sigma_S}(T_B - T_T)\right] \tag{11}$$

Using this very idealized solidification interface, we were able to derive a relation between the Seebeck signal and some important characteristics of the cellular structure. However, to build the connection with the experimental data, a more realistic cell model would be necessary.

The contribution of the tip temperature $(T_T - T_{eq})$ can be easily determined solving the diffusion equation along with the boundary condition defining the solute gradient at the interface as $\overline{G}/m_L$. The tip undercooling is thus found to decrease with interface velocity as $D\overline{G}/V_l$. An estimation of the other term on the right hand side of eq. (11) is more difficult: indeed, both the temperature difference along the structure and the equivalent liquid fraction depend on the characteristics of the cellular growth model.

At this preliminary stage of the analysis, we tried to fit the experimental data obtained during the USMP-1 mission using a simple $D\overline{G}/V_l$ power law. The result, presented in fig. 9, clearly show that the tip undercooling alone can not account for the observed signal. The structure dependent contribution in eq. 11) is thus seen to play a significant role, and more work on this point is now necessary to estimate its value.

CONCLUDING REMARKS

All the results presented in this paper are based on the analysis of the undercooling signal. Since the correlation between the Seebeck and a posteriori concentration measurements in the solid phase was seen to be good in ground based experiments [1], we are confident that these preliminary conclusions are valid. Of course, the metallographic processing of our space samples - currently under way - will also provide additional valuable information.

Concerning the planar front solidification, it can be safely said that mass transport in the fluid phase was mainly diffusive during the flight. However, transient g jitters effects were observed; after

such perturbations, the return to the steady state was seen to be very slow. Along with the analysis of the correlation between accelerometric and undercooling data, an important modeling effort is necessary to understand the relevant transport mechanisms involved.

A tentative interpretation of the Seebeck signal in cellular growth, based on the approximate integration of the local thermoelectricity equation in the vicinity of a squared waved interface, was also proposed. Further work on the topic will feature an estimation of the structure dependent contribution using more realistic cellular models. Finally, the morphological stability threshold will be precise thanks to the experimental data.

ACKNOWLEDGMENTS

REFERENCES

1. A. Rouzaud, J. Comera, P. Contamin, B. Angelier, F. Herbillon and J.J. Favier, J. Crystal Growth, 129 (1993) 173.

2. A. Rouzaud, J.J. Favier and D. Thevenard, Adv. Space Res., 8 (1988) 49.

3. C.C. Lin and L.A. Segel, Mathematics Applied to Deterministic problems in the Material Sciences, Macmillan (1974).

4. J. P. Garandet, T. Duffar and J.J. Favier, J. Crystal Growth, 106 (1990) 437.

5. J. P. Garandet, A. Rouzaud, T. Duffar and D. Camel, J. Crystal Growth, 113 (1991) 587.

6. S. Kaddeche, H. Ben Hadid and D. Henry, submitted to J. Crystal Growth.

7. J. P. Garandet, J.J. Favier and D. Camel, J. Crystal Growth, 130 (1993) 122.

8. A. Rouzaud, J. Crystal Growth.

9. J. I. D. Alexander, J. Ouazzani and F. Rosenberger, J. Crystal Growth, 97 (1989) 285.

10. J. I. D. Alexander, S. Amiroudine, J. Ouazzani and F. Rosenberger, J. Crystal Growth, 113 (1991) 21.

11. J. W. Rutter and B. Chalmers, Can. J. Phys., 31 (1953) 15.

12. W.W. Mullins and R.F. Sekerka, J. Appl. Phys., 34 (1963) 323.

13. S. R. Coriell, D.T.J. Hurle and R.F. Sekerka, J. Crystal Growth, 32 (1976) 1.

14. J. J. Favier and A. Rouzaud, J. Crystal Growth, 64 (1983) 367.

15. T. Alboussiere, R. Moreau and D. Camel, C.R. Acad. Sci. Paris, 313 II, (1991) 749.

Table 1

Physicochemical Parameters and Nominal Growth Conditions during the USMP-1 mission

Thermal expansion coefficient : $\beta_T = 10^{-4}$ K

Kinematic viscosity : $\nu = 2.6 \times 10^{-7}$ m^2 s^{-1}

Bi diffusion coefficient : $D = 1.8 \times 10^{-9}$ m^2 s^{-1}

Partition coefficient : $k = 0.29$

Liquidus slope : $m_L = -2.2$ K(at% Bi)$^{-1}$

Electrical conductivity :

           liquid : $\sigma_L = 2.15 \times 10^6$ Ω^{-1} m^{-1}

           solid : $\sigma_S = 4.3 \times 10^6$ Ω^{-1} m^{-1}

Global thermoelectric power : $\eta_S - \eta_L = 1.6 \times 10^{-6}$ V K^{-1}

Nominal concentration : $C_0 = 0.5$ at% Bi

Sample diameter : $H = 6 \times 10^{-3}$ m

Thermal gradient :

           liquid : $G_L = 13.5 \times 10^3$ Km^{-1}

           solid : $G_S = 6.75 \times 10^3$ Km^{-1}

Growth velocity : V_I $2 \rightarrow 27 \times 10^{-6}$ ms^{-1}
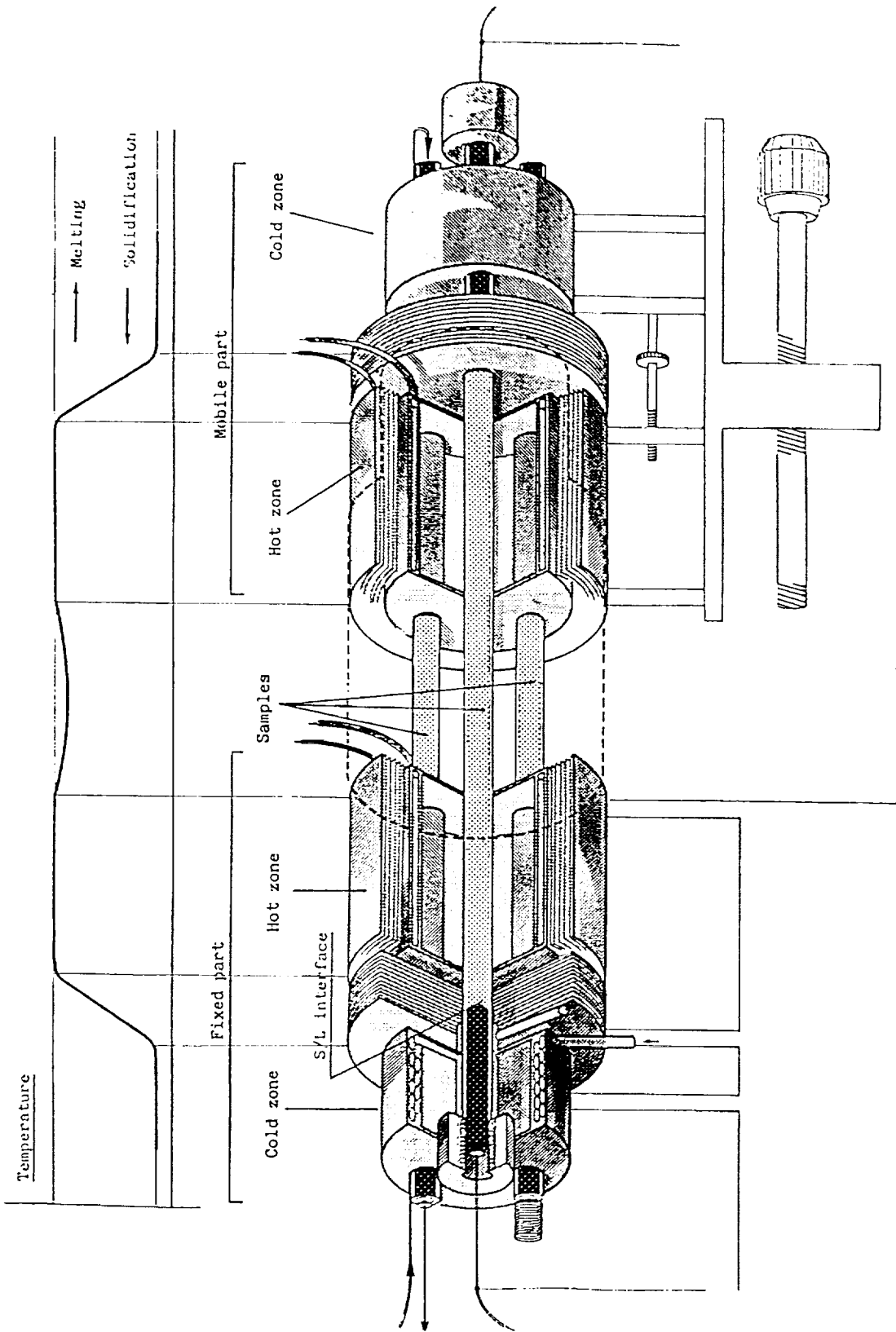
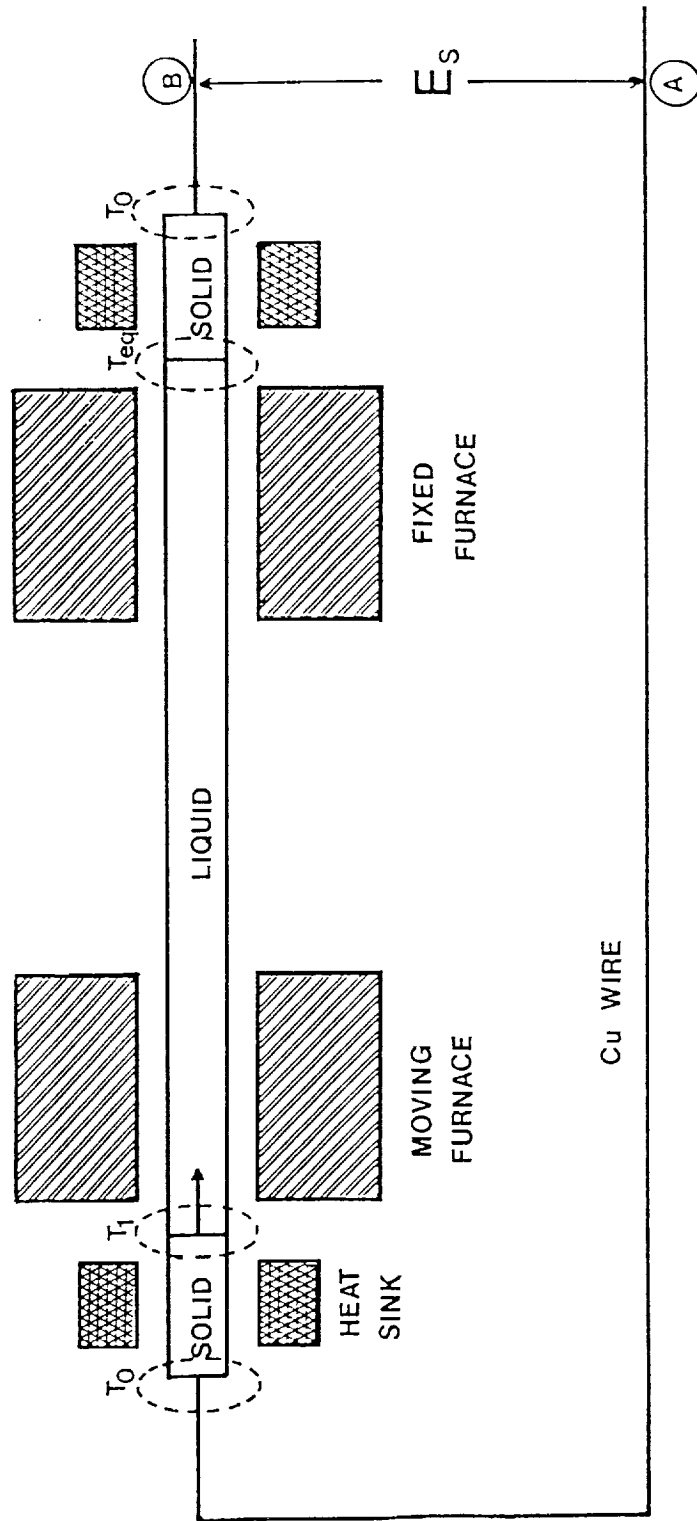Figure 1 Schematic of MEPHISTO.

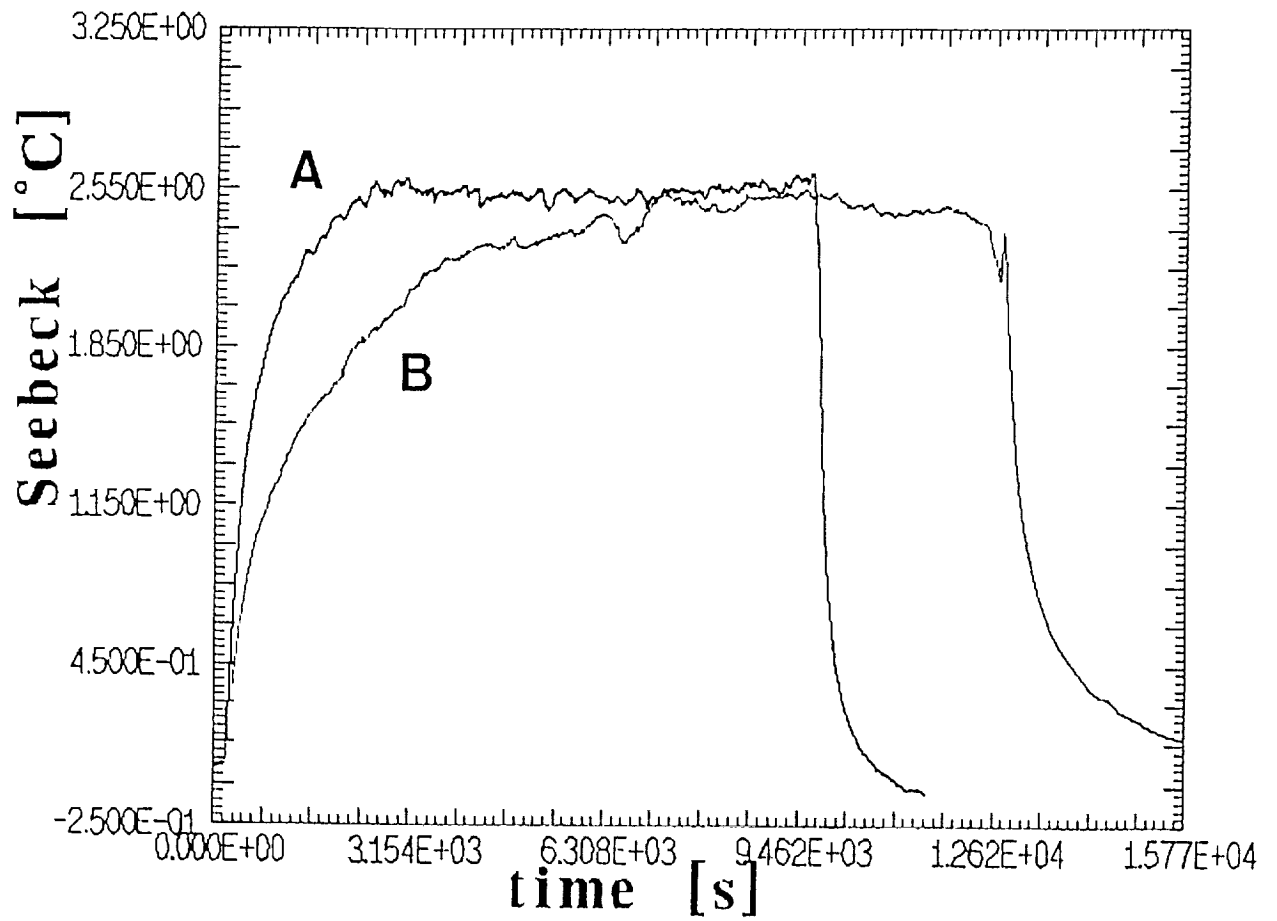Figure 2   Seebeck thermoelectric loop featuring the two solid-liquid interfaces.

Figure 3   Typical planar front solidification Seebeck signals with interface velocities of 5.2 μm/s (A) and 2 μm/s (B).
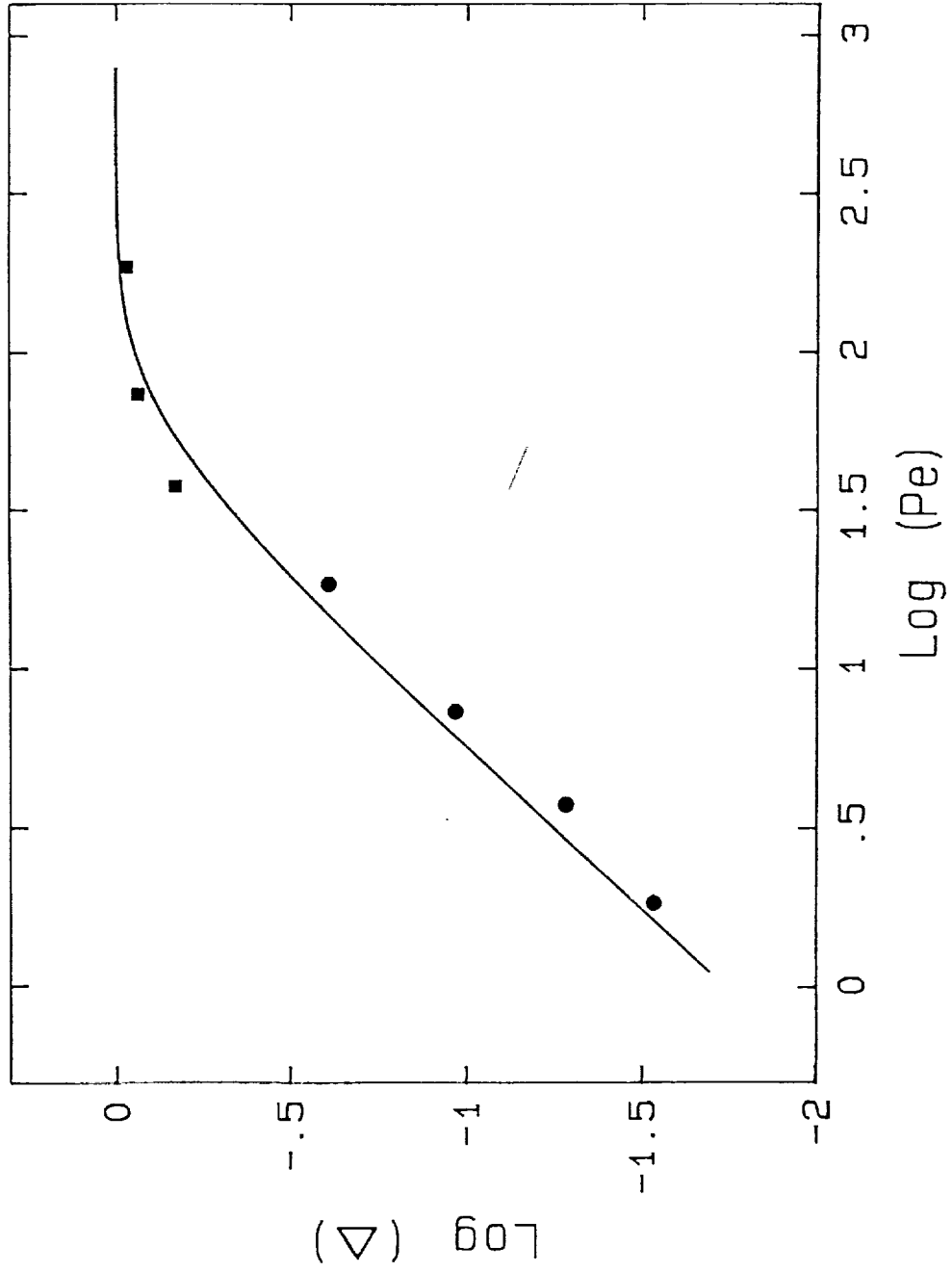
Figure 4 Variation of the experimental (symbols) and calculated (curve) values of the convecto-diffusive parameter Δ with the Peclet number.
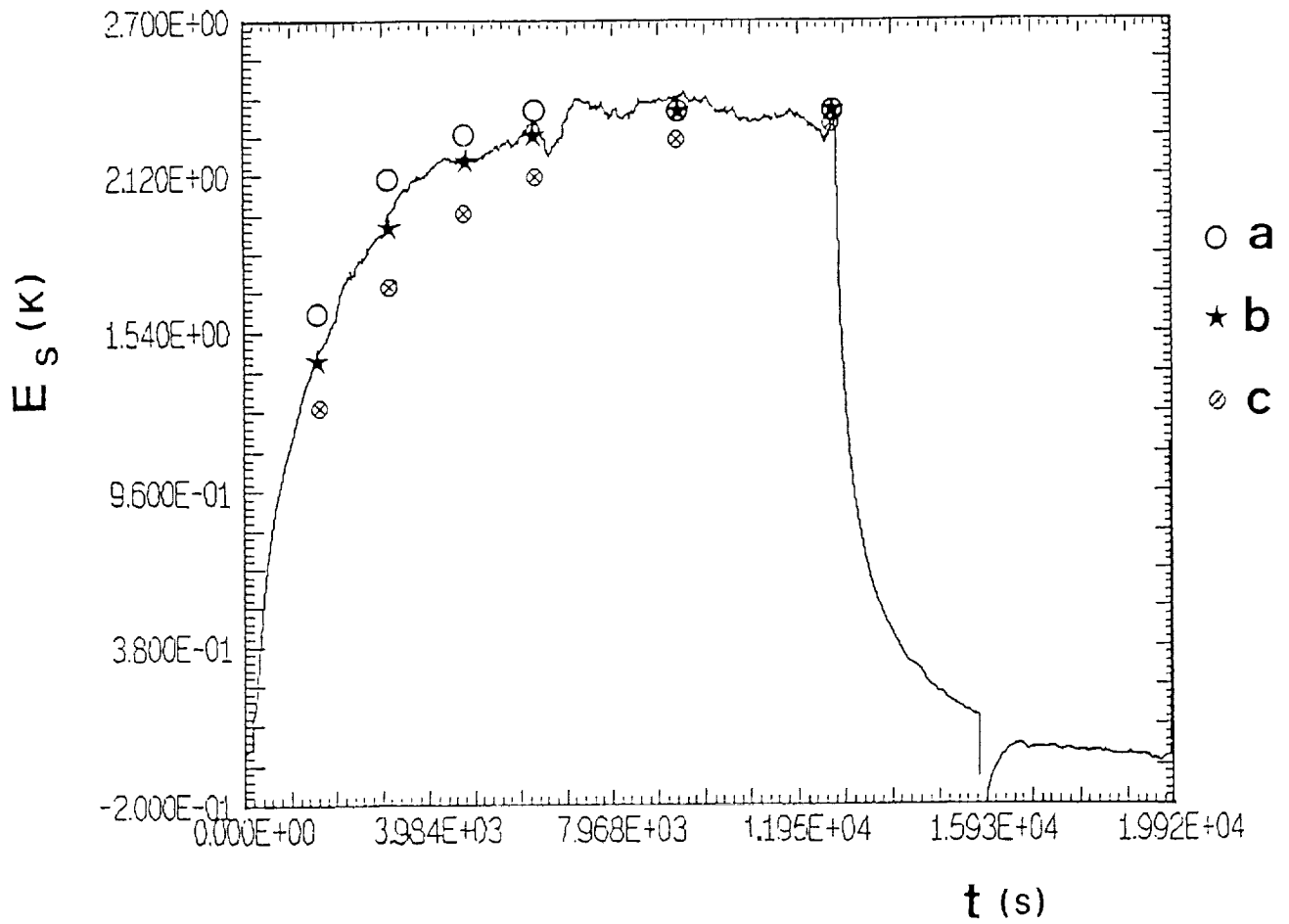
Figure 5 Fit of the observed Seebeck signal assuming negligible mass transport, with diffusion coefficients of 1.2 $\times 10^{-9}$ m^2s^{-1} (a), 1.8 $\times 10^{-9}$ m^2s^{-1} (b) and 2.5 $\times 10^{-9}$ m^2s^{-1} (c).
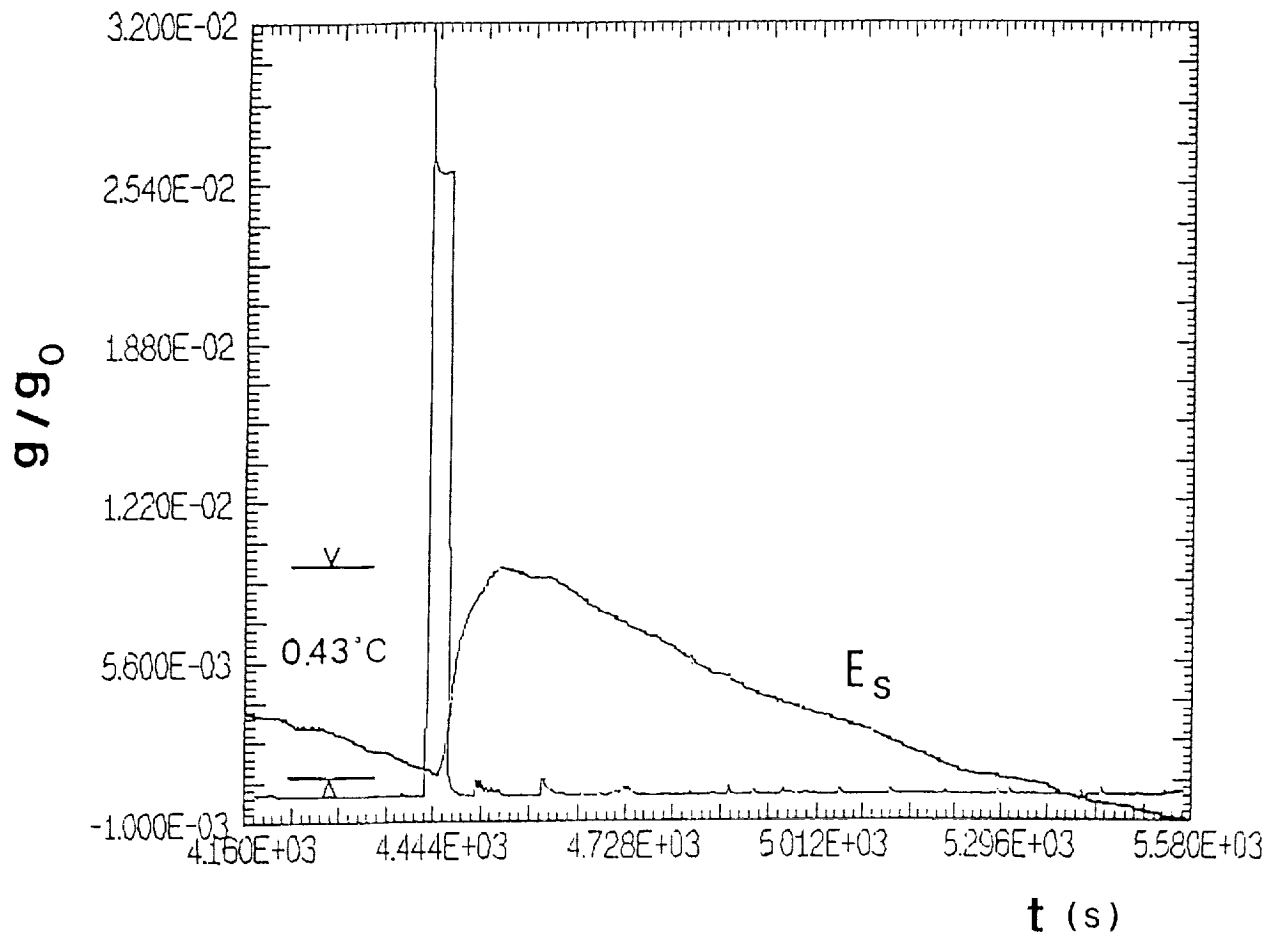
Figure 6   Effect of a major gravity perturbation (OMS burn) on the Seebeck signal E_S.
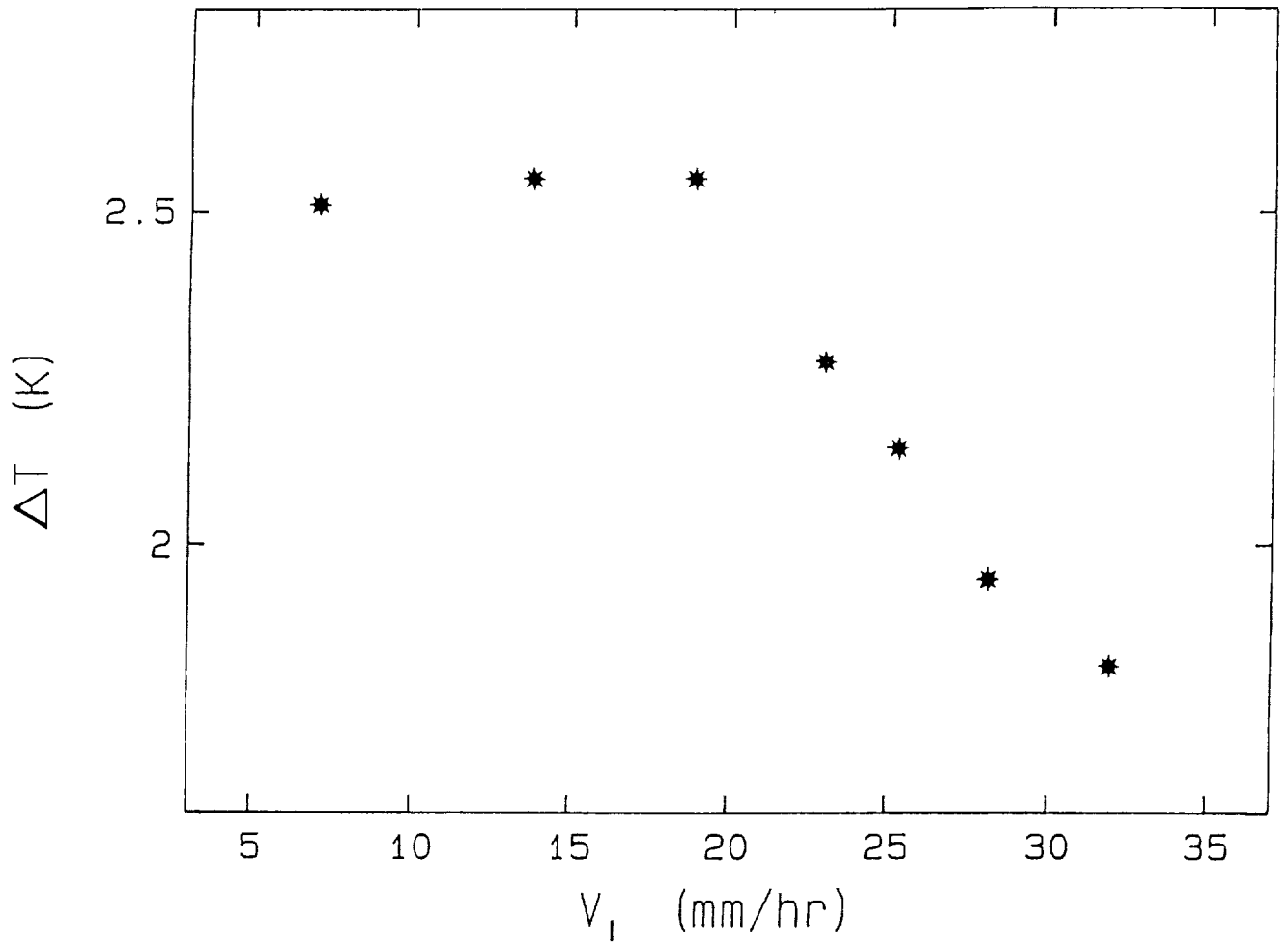
Figure 7 Variation of the experimentally observed undercooling around the morphological stability threshold.
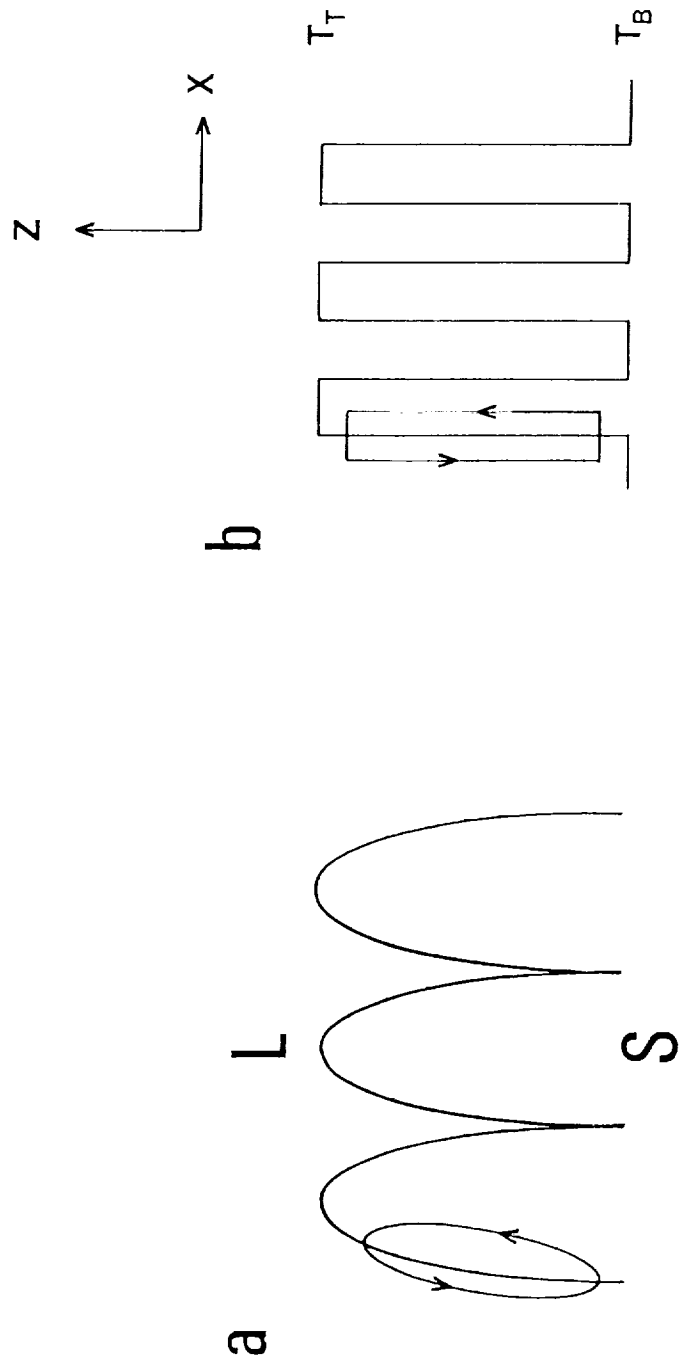
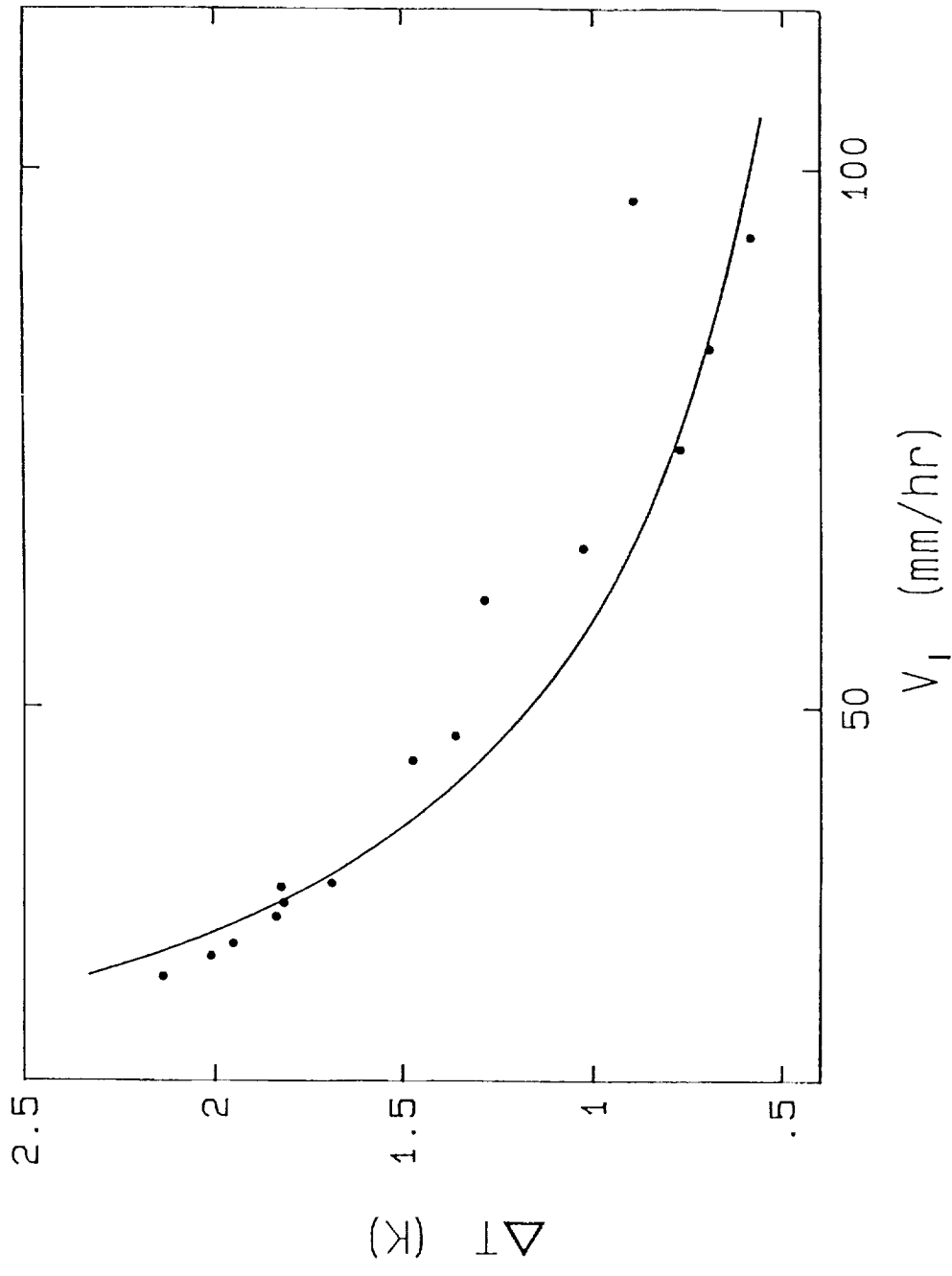Figure 8   Actual (a) and model (b) cellular interfaces.

Figure 9 Variation of the experimental (symbols) and calculated (curve) undercoolings as a function of the growth velocity for cellular interfaces.

Discussion

Question: *In one of your charts, it appears as though higher velocities are present in some regions of the wall. Is that just an illusion or is that real?*

Answer: Our samples were put in quartz crucibles, and in order to get wetting of the crucible by the samples we design a specific roughness in the inner part of the of the wall. This ensures a contact between the liquid at any time and the quartz crucible. Again just sufficient contact with the wall only because afterwards we should be able to pull out the sample from the crucible. Maybe this is the illusion you got from the pictures of some of the morphologies.

Question: *Following up, then you are saying that the samples remained of constant diameter ?*

Answer: Yes. Except in the middle part of the sample between the two furnaces. We had two furnaces, so at the very end of the solidification we just shut down the furnaces and the middle part was just solidified without directional solidification. In that part we got some variation of the diameter of the sample.

Question: *It has been known for a long time that the morphological instabilities in these dilute alloys for these rough interface materials is a sub critical bifurcation; so this is induced by grain boundaries or the edges of the sample. Is the sub critical nature of these bifurcations taken into account?*

Answer: Yes. In this slide, you can see that the perturbation occurs in a specific region here and here which are in fact the regions where we had the grain boundaries in the cross sections.

Question: *Right. I am just asking, you compared it to what you called theory, does that theory take into account the presence of an initial grain boundary groove?*

Answer: No. It does not.